MICROSTRUCTURAL EVIDENCE FOR THE CONDENSATION ORIGIN OF HIBONITE-SPINEL INCLUSIONS FROM ALH A77307 (CO3.0). Jangmi Han[1,2], Lindsay P. Keller[2], and Adrian J. Brearley[3]. [1]Lunar and Planetary Institute, Houston, TX 77058, USA (jangmi.han@nasa.gov); [2]ARES, NASA/JSC, Houston, TX 77058, USA; [3]Department of Earth and Planetary Sciences, MSC03-2040, University of New Mexico, Albuquerque, NM 87131, USA.

Introduction: Hibonite is a highly refractory phase occurring in many CAIs and Wark-Lovering rims from different chondrite groups [1]. Hibonite is predicted to be one of the earliest refractory phases to form by equilibrium condensation from a cooling gas of solar composition [2]. Therefore, hibonite can provide important insights into the earliest stages of solar nebular evolution.

A previous FIB/TEM study of a hibonite-spinel CAI in ALH A77307 (CO3.0) presented the crystallographic relationship between hibonite and spinel, suggesting that their structural similarity caused kinetic inhibition of melilite condensation and instead favored epitaxial nucleation and growth of spinel on the hibonite surfaces [3]. Here, we present the microstructures of two hibonite-spinel CAIs in ALH A77307 using FIB/TEM techniques to better understand their formation conditions and processes.

Methods: Each FIB section of two hibonite-spinel CAIs in ALH A77307 was extracted from a region consisting of subparallel hibonite laths intergrown with spinel and minor perovskite. These FIB sections were cut normal to the elongation direction of the hibonite laths [3,4]. The FIB sections were investigated in detail using a variety of TEM techniques (BF- and HR-TEM, STEM, EDS, and electron diffraction).

Results: Two hibonite-spinel CAIs (03 and 08) in ALH A77307 share characteristics common to this type of CAI [3,5]: (1) they are irregularly-shaped, porous objects with a small size of 70×40 μm for 03 and 55×50 μm for 08, (2) lath-shaped hibonite grains 3-40 μm long and 0.3-9 μm wide are embedded in spinel and are subparallel to each other, and (3) fine-grained, subrounded to elongated perovskite grains with a size of 0.2-4 μm commonly occur as inclusions in spinel and often in hibonite. In contrast, only CAI 03 contains melilite, but CAI 08 is melilite free.

Both FIB sections (03-A and 08-A) consist mainly of hibonite and spinel with minor perovskite inclusions. Individual mineral constituents have similar microstructures. Hibonite grains are typically lath-shaped and intergrown with each other. Hibonite grains show various thicknesses and lengths; 0.2-5 μm long and 60 nm-2.5 μm wide in 03-A and 2-11 μm long and 0.5-6.5 μm wide in 08-A. Electron diffraction patterns of hibonite grains reveal that the grains are consistently elongated along the *a* axis, but have different orientations relative to one another. Spinel is usually irregularly-shaped with a size of 0.5-3.5 μm in 03-A and 1-6.5 μm in 08-A. Perovskite inclusions (0.2-5 μm in size) in hibonite and spinel are subrounded to elongated. In addition, FIB 03-A contains elongated melilite (0.2-2 μm long) interstitial to hibonite laths.

While spinel and perovskite are relatively featureless and free of defects, most hibonite grains in both FIB sections contain numerous planar defects; however, the concentration of planar defects varies among and within the hibonite grains. Electron diffraction patterns of hibonite show weak streaking along *c**, indicating stacking disorder. As shown in Figure 1, HR-TEM images of hibonite grains show variations in spacing of the lattice fringes, suggestive of stacking disorder. In most cases, isolated layers that are 1.6 nm wide are randomly intergrown with the prominent 1.1 nm wide (002) layers of stoichiometric hibonite. We also observe more complex intergrowth combinations. We observe the intergrowth of 7 nm wide layers with the 2.2 nm wide layers of stoichiometric hibonite. The most complex case is the intergrowth of layers of various spacings ranging in width from 4.8 to 11.4 nm with the 2.2 nm wide layers of stoichiometric hibonite. Analytical electron microscopy shows that hibonite grains are close to $Ca(Al,Si,Ti,Mg)_{12}O_{19}$ in composition, but show Ca deficiencies by up to ~10 mol% where the defects are concentrated.

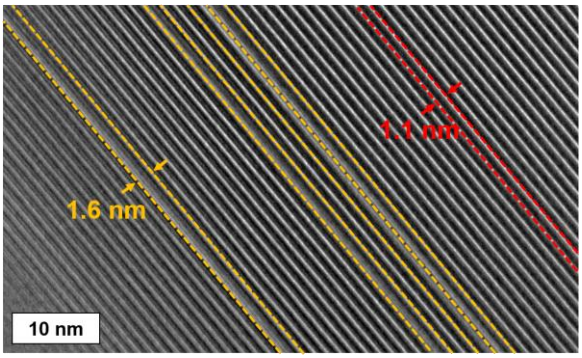

Figure 1. HR-TEM image of hibonite from FIB 03-A. The 1.6 nm wide layers (yellow dashed lines) are randomly distributed in ordered regions with the 1.1 nm wide layers (red dashed lines).

Discussion: Our overall petrologic and mineralogical observations from two hibonite-spinel CAIs in ALH A77307 are generally consistent with the predictions of mineral formation from equilibrium condensation calculations [2]. The irregular shapes and porous textures

of these CAIs also support a condensation origin. It is therefore very likely that hibonite formed by high-temperature condensation from a nebular gas, followed by perovskite and spinel.

Textural relationships in the hibonite-spinel CAIs, however, indicate that spinel, rather than melilite, condensed following hibonite condensation, inconsistent with equilibrium condensation calculations [2]. This suggests that conditions of condensation for these CAIs departed from thermodynamic equilibrium. Melilite condensation was extremely limited, demonstrated by its rarity in both CAIs. Instead, the occurrence of spinel in crystallographic continuity with hibonite demonstrates that spinel condensed directly onto hibonite. Epitaxial nucleation and growth of spinel may have occurred on the surfaces of hibonite, probably due to the lower activation energy for spinel nucleation compared with that of melilite [3].

The presence of perovskite inclusions within hibonite may be attributed to simultaneous condensation of these phases over a limited temperature interval [2]. Early-condensed hibonite grains trapped adjacent condensing fine-grained perovskite grains and continued to nucleate and grow into larger crystals. As nebular cooling proceeded, hibonite condensation eventually ceased, but perovskite kept condensing and was later enclosed by spinel once spinel condensation commenced at lower temperatures [3].

The presence of planar defects in hibonite provide useful insights into possible formation conditions of these two CAIs. Ideal hibonite consists of a sequence of four-closely-packed O layers and Al ions in a spinel block (S) alternating with a Ca-containing layer (C), resulting in a unit cell containing 2 (S+C) blocks (S+C+S+C) [6]. The observed 1.1 nm wide lattice fringes correspond to the *c* dimension of the ideal hibonite structure consisting of one basic structural unit representing the combination of a spinel block and a Ca-containing layer (S+C) [6]. The local presence of 1.6 nm wide lattice fringes can be interpreted as the result of modification of the stacking sequence due to the presence of a thicker spinel block with six ccp O layers (S+S+C) [6]. Therefore, the observed wide range of spacings can be interpreted as different stacking combinations of the basic structural spinel block versus the Ca-containing layer. This interpretation is consistent with the observed Ca deficiency of hibonite.

There are three possible explanations for the Ca deficiency of hibonite; (1) reheating and partial evaporation of Ca from hibonite, (2) equilibrium condensation of Al-rich spinel in hibonite, and (3) non-equilibrium condensation of hibonite and (S+S+C) phase. Evaporative loss of Ca from hibonite may have occurred during or after hibonite condensation as a result of later reheating. Calcium loss requires extensive evaporation, resulting in complete loss of moderately refractory elements (e.g., Mg). Therefore, Mg isotopic mass dependent fractionation is expected without Ca isotopic mass dependent fractionation [7]. However, the absence of any Mg isotopic mass dependent fractionation from similar hibonite-bearing CAIs in CO3 chondrites [5,8] appears to rule out evaporation as an important mechanism, although Mg isotopic data for the CAIs in this study are lacking.

Second, Al-rich spinel may have condensed as isolated layers within hibonite. A thermodynamic mixing model for the spinel $MgAl_2O_4$-$Al_{8/3}O_4$ solid solution suggests that Al-rich spinel is stable between 1,920-2,267 K [9]. However, equilibrium condensation calculations predict that, at these temperatures, Al-rich spinel fails to condense due to dominant Al and Ca condensation, instead forming Ca-aluminates or liquids in dust-enriched systems [10].

However, the lack of melilite in these CAIs indicates that they did not form at equilibrium. Based on the observations, we propose that the intergrowth of hibonite and the (S+S+C) phase is the product of formation under non-equilibrium conditions, where the formation of the defect-structured hibonite is energetically more favorable than corundum formation by direct condensation. Under non-equilibrium conditions, corundum condensation may be inhibited. Excess Al in the gas phase was incorporated into the hibonite as extra spinel blocks, resulting in the planar defects with the (S+S+C) stacking sequence.

Conclusions: Our TEM observations suggest that two hibonite-spinel CAIs in ALH A77307 formed by high-temperature condensation from the cooling solar nebula under non-equilibrium conditions. The planar defects in hibonite may have formed by the accommodation of some excess Al into the hibonite in the form of the extra spinel blocks. Interestingly, similar microstructures are also observed in hibonites from Wark-Lovering rims [11], indicating the common formation histories for the different occurrences of hibonite.

Acknowledgements: This research was supported by NNX11AK51G to A.J. Brearley (PI) and 10-COS10-0049 to L.P. Keller (PI).

References: [1] MacPherson G.J. (2014) Treatise on Geochemistry II vol.1 pp.139-179. [2] Ebel D.S. (2006) MESS2 pp.253-277. [3] Han J. & Brearley A.J. (2014) *LPS XLV,* Abstract #2125. [4] Han J. et al. (2014) *MAPS, 49,* A151. [5] Russell S.S. et al. (1998) *GCA, 62,* 689-714. [6] Schmid H. & De Jonghe L.C. (1983) *Philos. Mag. A, 48,* 287-297. [7] Simon J.I. & DePaolo D.J. (2010) *EPSL, 289,* 457-466. [8] Fahey A.J. et al. (1994) *GCA, 58,* 4779-4793. [9] Sack R.O. (2014) *Am. J. Sci., 314,* 858-877. [10] Ebel D.S. et al. (2014) *MAPS, 49,* A101. [11] Keller L.P. (1991) *AGU, 72,* 141.